*Thermophysics and Aeromechanics*, *2016*, *Vol. 23*, *No. 4*

DOI: 10.1134/S0869864316040089

# Mathematical simulation of melting inside a square cavity with a local heat source*

**N.S. Bondareva[1] and M.A. Sheremet[1,2]**

[1]*Tomsk State University*, *Tomsk*, *Russia*

[2]*Tomsk Polytechnic University*, *Tomsk*, *Russia*

E-mail: Michael-sher@yandex.ru

(*Received October 30*, *2015*; *in revised form November 29*, *2015*)

Numerical simulation of transient melting regimes inside an enclosure in the presence of a local heat source has been carried out. Mathematical model formulated in terms of dimensionless variables such as stream function, vorticity, and temperature has been numerically solved by finite difference method. Effects of the Rayleigh number $4 \cdot 10^5 \le Ra \le 5 \cdot 10^7$, Stefan number $2.21 \le Ste \le 5.53$, and dimensionless time on velocity and temperature fields as well as on the local Nusselt number along the heat source surface have been analyzed in detail. The transient effects of the considered process at high values of the Rayleigh number have been identified.

**Key words:** melting, natural convection, heat conduction, Boussinesq approximation, laminar regime, numerical simulation.

The phase-change materials (alkanes, fatty acids, saline solutions) enjoy in recent years wide application in power engineering [1]. These substances have, as a rule, a relatively low temperature of melting, high latent energy of melting, and high heat capacity. The energy absorption and heat release at the expense of phase changes is used at the cooling of electronics, in solar power storage devices, systems of thermal regulation in buildings, which is explained by the property of such materials to absorb and release a large amount of energy whereas retaining the temperature nearly invariable and performing concurrently the phase change.

A few works have been published by now, which are devoted to the investigation of unsteady regimes of natural convection in regions filled with phase change materials (PCMs) [1–11]. So, for instance, the results of an experimental study of the pure gallium melting inside a parallelepiped with two isothermal opposite vertical faces and the adiabatic remaining walls are presented in the work [2]. The authors have succeeded in watching the evolution of the melting front and to establish the correlation relations for the heat exchange coefficient. It is to be noted that this work is frequently used as a sample at the development of computer codes for modeling the convective heat transfer with phase changes [3–8]. Numerical modelling of the regime of the melting of PCM (*n*-octadecane) inside a rectangular cavity with the isothermal lower wall and thermally insulated remaining boundaries was carried out in

* The work has been supported financially by the Russian Foundation for Basic Research (Grant No. 14-08-31137 mol_a) and the Council for Grants of the RF President for young Russian scientists (Grant MD-6942.2015.8).

the work [3]. As a result, the velocity and temperature distributions were obtained by the finite element method, which show the evolution of the melting process as well as the thermal and hydrodynamic structures were presented, which illustrate the influence of the Rayleigh number. The investigation of the process of melting of a solid gallium in a closed rectangular cavity in the presence of the isothermal sine-shaped wall has been presented in the work [4]. The modeling was carried out by the control volume method using an unstructured grid and the enthalpy-porous approach to the melting front identification. An increase in the melting intensity with increasing amplitude of the curved boundary due to a growth of the area of contact between the isothermal boundary and the melting material was revealed. It is to be noted that the use of wavy surfaces in closed technological systems enables a considerable intensification of the heat transfer process [5]. An analysis of steady regimes of natural convection in the presence of phase changes in a closed differentially heated square cavity [6] has shown a significant dependence of the scales and intensity of the internal convective flow as well as the phase boundary shape on Rayleigh, Prandtl, and Stefan numbers. In particular, it was found that an increase in the Rayleigh number leads to a considerable curvature of the interphase boundary.

A number of studies [7–11] were devoted to the development of an efficient system for cooling the electronic devices with the use of PCMs. The experimental investigation of the conditions for cooling the portable electronic devices based on PCMs, which are placed inside the heat removal zone, was carried out in the works [7, 8]. As a result, it was found that the use of the *n*-eikosane inside the aluminum structure for heat removal enables one to stabilize the temperature of the entire system and increases the device lifetime. It is to be noted that the latter depends on the volume of the employed PCM and the power of the heat release source. An analysis of the efficiency of the aerial cooling system for telecommunication base stations using PCMs has been presented in the work [9]. The internal space of base stations was cooled at the expense of the conditioning of cold air masses of the ambient medium, and the excessive energy of cooling was accumulated in the containers filled with PCM. At the switch-off of the system for the room conditioning, the cooling was performed at the expense of phase changes inside the containers. It was shown that such a system enables a substantial reduction of the amount of the electric power consumption, in some regions, up to 67 %. Numerical modeling of three-dimensional unsteady regimes of cooling a portable electronic device using PCMs was conducted in the works [10, 11]. It was found that the partition of the entire volume of PCM into several parts with the aid of heat-conducting diaphragms enables one to intensify the cooling regime and to stabilize the temperature inside the device itself during a long time.

The above overview has shown that the published results reflect only the influence of infinitely thin isothermal elements, which are located along the boundaries of the region under analysis, on the flow structure and heat transfer inside the cavity as a result of the work medium melting. The presence of local isothermal elements of finite sizes is known to lead even in the case of the thermogravitational convection of the aerial medium to a substantial modification of hydrodynamic fields inside the cavity and manifests itself in the alteration of the intensity of heat removal from the surface of such heat-releasing elements [12]. It is necessary to conduct further research for a detailed study of the influence of local heat-releasing elements on melting regimes.

The purpose of the present work is the numerical analysis of unsteady regimes of the melting of PCM inside an enclosure with a local energy source of square shape, which is located at the lower boundary, and the vertical cooling walls. Unlike the works presented in the overview, the modeling is performed in the proposed study by using the transformed variables “stream function – vorticity – temperature”, which enables a substantial CPU time reduction at the expense of reducing the number of equations to be solved.

**Mathematical model and solution method**

The unsteady process of the material melting inside a square enclosure in the presence of an isothermal source with temperature $T_h$ (Fig. 1) is considered. The solution region contains two vertical isothermal boundaries with temperature $T_w$ ($T_h > T_w$), the remaining walls are adiabatic. The heat supply to the region is carried out at the expense of a square source, which lies on the lower wall and has a constant temperature above the material melting temperature. At the initial moment of time, the material is in solid state and has the temperature equal to the material melting temperature $T_m$. It is assumed at the execution of numerical experiments that the heat transfer realizes inside the working medium at the expense of the heat conduction and convection mechanisms; the melt is a Newtonian fluid satisfying the Boussinesq approximation; the melt flow regime is laminar; one can neglect the viscous dissipation; the enclosure walls are impermeable for the melt.

The process of the transfer of mass, momentum, and energy is described by the system of the Oberbeck–Boussinesq unsteady two-dimensional convection equations in natural variables "velocity–pressure–enthalpy" [11, 13]:

$$\frac{\partial u}{\partial x}+\frac{\partial v}{\partial y}=0, \tag{1}$$

$$\frac{\partial u}{\partial t}+u\frac{\partial u}{\partial x}+v\frac{\partial u}{\partial y}=-\frac{1}{\rho}\frac{\partial p}{\partial x}+\nu\left(\frac{\partial^2 u}{\partial x^2}+\frac{\partial^2 u}{\partial y^2}\right), \tag{2}$$

$$\frac{\partial v}{\partial t}+u\frac{\partial v}{\partial x}+v\frac{\partial v}{\partial y}=-\frac{1}{\rho}\frac{\partial p}{\partial y}+\nu\left(\frac{\partial^2 v}{\partial x^2}+\frac{\partial^2 v}{\partial y^2}\right)+g\beta\left(T-T_f\right). \tag{3}$$

The energy equation is written in the enthalpy form:

$$\frac{\partial h}{\partial t}+u\frac{\partial h}{\partial x}+v\frac{\partial h}{\partial y}=\lambda\left(\frac{\partial^2 T}{\partial x^2}+\frac{\partial^2 T}{\partial y^2}\right), \tag{4}$$

where $h=\begin{cases}\rho_s C_s T, & T<T_m,\\ \rho_s C_s T_m+\rho_m L_m+\rho_m C_m\left(T-T_m\right), & T\ge T_m.\end{cases}$ Here $g$ is the acceleration due to gravity, $\beta$ is the thermal coefficient of volumetric expansion, $x$ and $y$ are the coordinates of a Cartesian coordinate system, $\rho_s$ is the density of the material in its solid state, $\rho_m$ is the melt density, $C_s$ is the specific heat of the material in its solid sate, $C_m$ is the melt specific heat, $u$ and $v$ are the velocity vector components in projection onto the $x$ and $y$ axes, respectively, $t$ is the time, $p$ is the pressure, $\nu$ is the kinematic coefficient of viscosity, $h$ is the enthalpy, $\lambda$ is the thermal conductivity coefficient, $L_m$ is the latent heat of melting.

To eliminate the discontinuity of the enthalpy as a function of temperature the smoothing mapping was introduced at the interface [13, 14]:

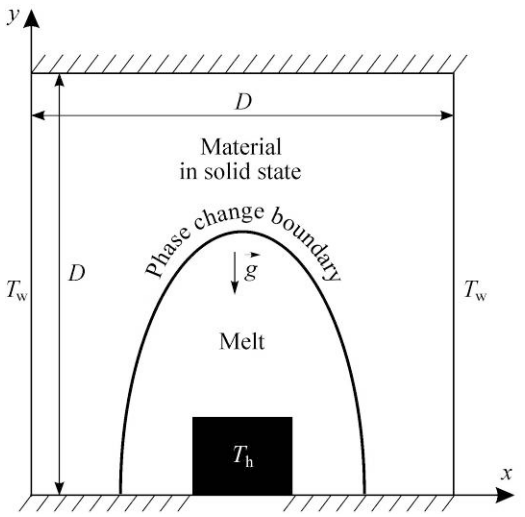


*Fig. 1.* Solution domain of the problem.

$$\varphi = \begin{cases} 0, & T < T_{\mathrm{m}} - \eta, \\ \dfrac{T - (T_{\mathrm{m}} - \eta)}{2\eta}, & T_{\mathrm{m}} - \eta \le T \le T_{\mathrm{m}} + \eta, \\ 1, & T > T_{\mathrm{m}} + \eta, \end{cases} \tag{5}$$

where $\eta$ is the transition zone size near the interphase boundary. The control parameter value $\eta$ was determined from numerical experiments [13, 14].

The introduction of the smoothing function (5) reflects the presence of a transitional zone in the interphase boundary neighborhood and enables thereby a passage from the equation for the enthalpy (4) to the equation for temperature and no separation of the regions of the liquid and solid phases by solving the obtained energy equation by a homogeneous method [11, 13, 14].

To reduce the CPU time at the solution of the problem under consideration, the stream function $\psi$ $\left(u = \dfrac{\partial \psi}{\partial y},\ v = -\dfrac{\partial \psi}{\partial x}\right)$ and the vorticity $\omega$ $\left(\omega = \dfrac{\partial v}{\partial x} - \dfrac{\partial u}{\partial y}\right)$ are introduced as the sought hydrodynamic functions. It is to be noted that the introduction of these functions enables one to eliminate from the consideration the pressure field and reduce thereby the number of the equations to be solved owing to the identical satisfaction of the continuity equation (1).

Numerical realization of the melting process was done in dimensionless variables. As the reference values for the distance, velocity, time, temperature, stream function, and vorticity the following values were chosen: $D$, $\sqrt{g\beta(T_{\mathrm{h}} - T_{\mathrm{m}})D}$, $\sqrt{D/\left[g\beta(T_{\mathrm{h}} - T_{\mathrm{m}})\right]}$, $(T_{\mathrm{h}} - T_{\mathrm{m}})$, $\sqrt{g\beta(T_{\mathrm{h}} - T_{\mathrm{m}})D^3}$, $\sqrt{g\beta(T_{\mathrm{h}} - T_{\mathrm{m}})/D}$, respectively. The dimensionless variables were as follows:

$$X = x/D,\ Y = y/D,\ U = u\Big/\sqrt{g\beta(T_{\mathrm{h}} - T_{\mathrm{m}})D},\ V = v\Big/\sqrt{g\beta(T_{\mathrm{h}} - T_{\mathrm{m}})D},$$
$$\tau = t\sqrt{g\beta(T_{\mathrm{h}} - T_{\mathrm{m}})/D},\ \Theta = (T - T_{\mathrm{m}})/(T_{\mathrm{h}} - T_{\mathrm{m}}),\ \Psi = \psi\Big/\sqrt{g\beta(T_{\mathrm{h}} - T_{\mathrm{m}})D^3},$$
$$\Omega = \omega\sqrt{D/\left[g\beta(T_{\mathrm{h}} - T_{\mathrm{m}})\right]},$$

where $D$ is the cavity size (Fig. 1), $X$ and $Y$ are the dimensionless coordinates corresponding to the $x$ and $y$ coordinates; $U$ and $V$ are the dimensionless velocities corresponding to the velocities $u$ and $v$; $\tau$ is the dimensionless time, $\Theta$ is the dimensionless temperature, $\Psi$ is the dimensionless stream function, $\Omega$ is the dimensionless vorticity.

With regard for the introduction of the smoothing function (5), the stream function and the vorticity as well as the dimensionless variables the governing equations (1)–(4) take the following form [11, 13–15]:

$$\frac{\partial \Omega}{\partial \tau} + \frac{\partial \Psi}{\partial Y} \cdot \frac{\partial \Omega}{\partial X} - \frac{\partial \Psi}{\partial X} \cdot \frac{\partial \Omega}{\partial Y} = \sqrt{\frac{\mathrm{Pr}}{\mathrm{Ra}}} \left( \frac{\partial^2 \Omega}{\partial X^2} + \frac{\partial^2 \Omega}{\partial Y^2} \right) + \frac{\partial \Theta}{\partial X}, \tag{6}$$

$$\frac{\partial^2 \Psi}{\partial X^2} + \frac{\partial^2 \Psi}{\partial Y^2} = -\Omega, \tag{7}$$

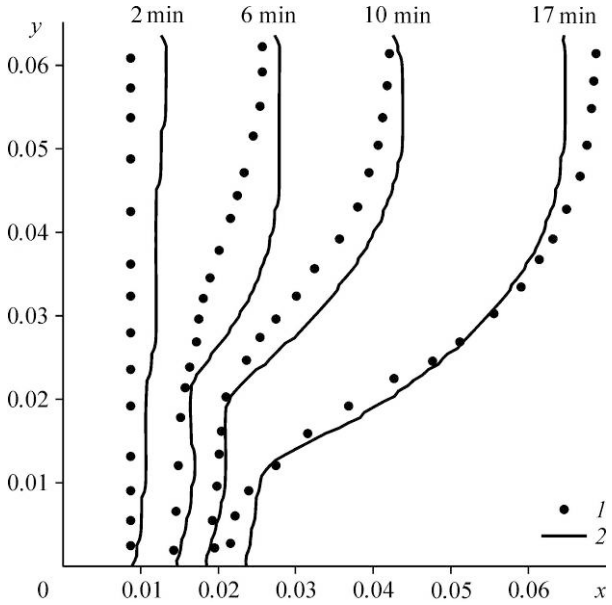


*Fig. 2.* Location of the melting front at different moments of time in comparison with experimental data of [2].
*1* — experimental data of [2], *2* — the computation.

$$\zeta(\varphi)\left[\frac{\partial\Theta}{\partial\tau}+\frac{\partial\Psi}{\partial Y}\cdot\frac{\partial\Theta}{\partial X}-\frac{\partial\Psi}{\partial X}\cdot\frac{\partial\Theta}{\partial Y}\right]+\mathrm{Ste}\cdot\left[\frac{\partial\varphi}{\partial\tau}+\frac{\partial\Psi}{\partial Y}\cdot\frac{\partial\varphi}{\partial X}-\frac{\partial\Psi}{\partial X}\cdot\frac{\partial\varphi}{\partial Y}\right]=$$
$$=\frac{\xi(\varphi)}{\sqrt{\mathrm{Ra}\cdot\mathrm{Pr}}}\left(\frac{\partial^2\Theta}{\partial X^2}+\frac{\partial^2\Theta}{\partial Y^2}\right), \tag{8}$$

here $\mathrm{Ra}=g\beta(T_\mathrm{h}-T_\mathrm{m})D^3/\nu a_\mathrm{m}$ is the Rayleigh number, $\mathrm{Pr}=\nu/a_\mathrm{m}$ is the Prandtl number, $\mathrm{Ste}=L_\mathrm{m}/C_\mathrm{m}(T_\mathrm{h}-T_\mathrm{m})$ is the Stefan number, $a_\mathrm{m}$ is the thermal diffusivity coefficient of the melt, $\zeta(\varphi)=\frac{\rho_\mathrm{s}C_\mathrm{s}}{\rho_\mathrm{m}C_\mathrm{m}}+\varphi\left(1-\frac{\rho_\mathrm{s}C_\mathrm{s}}{\rho_\mathrm{m}C_\mathrm{m}}\right)$ and $\xi(\varphi)=\frac{\lambda_\mathrm{s}}{\lambda_\mathrm{m}}+\varphi\left(1-\frac{\lambda_\mathrm{s}}{\lambda_\mathrm{m}}\right)$ are auxiliary functions.

It is to be noted that the auxiliary functions $\zeta(\varphi)$ and $\xi(\varphi)$ appear in equation (8) due to a passage from the energy equation in the enthalpy form to the energy equation written in terms of temperature. The use of the enthalpy form of the energy equation enables the application of a homogeneous method for determining the temperature field. Such an approach has been presented in more detail in the works [13, 14].

The initial and boundary conditions for the formulated system of partial differential equations (6)–(8) are as follows.

The initial condition: $\Psi(X,Y,0)=\Omega(X,Y,0)=\Theta(X,Y,0)=0$.

The boundary conditions:

– at the boundaries $X=0$ and $X=1$, the constant temperature of cooling $\Theta=\Theta_\mathrm{c}=-0.3$ is kept; in the case of the material melting up to the boundaries $X=0$ and $X=1$, the standard boundary conditions were considered for the stream function and vorticity: $\Psi=0$, $\Omega=-\partial^2\Psi/\partial X^2$;

– thermal insulation conditions $\partial\Theta/\partial Y=0$ were considered on horizontal walls; in the case of the material melting up to these boundaries, the conditions of the form $\Psi=0$, $\Omega=-\partial^2\Psi/\partial Y^2$ were considered for the stream function and vorticity;

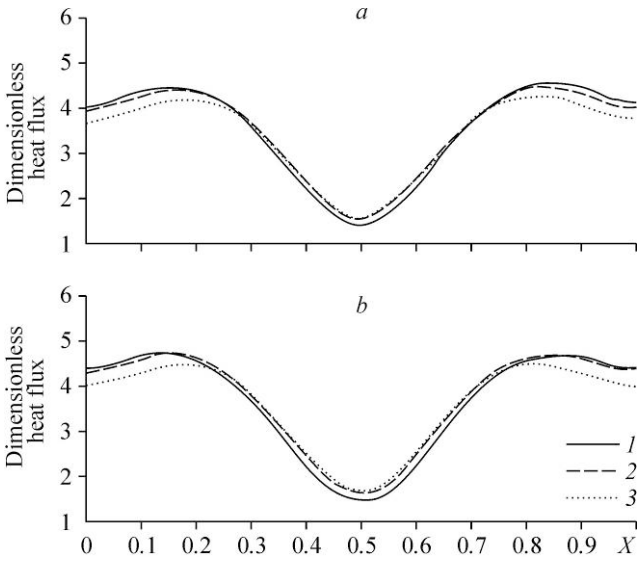


*Fig. 3.* Distributions of the local Nusselt number on the lower wall at different moments of time. The data of the work [3] (*a*) and the present work (*b*); $\tau$ = 709 (*1*), 851 (*2*), 1064 (*3*).

– at the interphase boundary: $\Psi = 0,\ \Omega = -\left(\partial^2\Psi/\partial X^2 + \partial^2\Psi/\partial Y^2\right)$;

– on the energy source surface: $\Theta = \Theta_h = 1,\ \Psi = 0,\ \Omega = -\left(\partial^2\Psi/\partial X^2 + \partial^2\Psi/\partial Y^2\right)$.

It is to be noted that at the initial moment of time ($\tau = 0$), the dimensionless temperature was equal to 0 in the entire region. At $\tau > 0$, the temperature $\Theta_c = -0.3$ was set immediately on the enclosure vertical walls, and on the energy source surface, the temperature $\Theta_h = 1$, which was just the source of heat transfer inside the enclosure.

The formulated boundary-value problem (6)–(8) with the corresponding initial and boundary conditions was solved by a finite difference method [12, 15–18] on a uniform structured grid of size 200×200. The Samarsky monotone second-order scheme [18] was used for

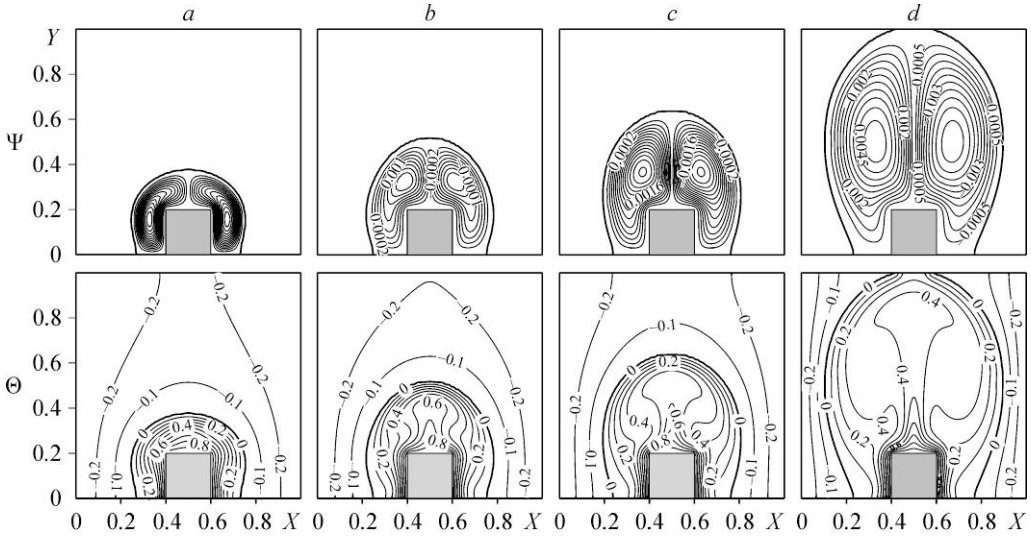


*Fig. 4.* Streamlines Ψ and isotherms Θ at Ra = $4\cdot10^5$ and Ste = 5.53. $\tau$ = 244.8 (*a*), 489.6 (*b*), 734.4 (*c*), and 1713.6 (*d*).

the discretization of convective terms in the equation for vorticity dispersion (6) and in the energy equation (8), and the diffusion terms were approximated in all equations by central differences. The Poisson difference equation for the stream function (7) was solved by the method of the successive over-relaxation. The equations of the vorticity dispersion and energy were approximated by using the locally one-dimensional Samarsky scheme. The obtained difference equations were solved by the Thomas method.

The developed solution method was tested on model problems [2, 3]. One can see in Fig. 2 a sufficiently close proximity of the melting front, which was obtained by the numerical method, with experimental data [2]. It is to be noted that the observed deviations in the phase change boundary at the initial time stage are due to a three-dimensional character of the problem as well as to some anisotropy of the pure gallium properties, which was used in experiment [2]. A more detailed description of the given test problem is presented in the work [16].

Figure 3 illustrates a good agreement of the profiles of the local dimensionless heat flux on the bottom isothermal wall versus time with the numerical data of [3]. The moments of time shown in Fig. 3*b* are identical with the moments of time in Fig. 3*a*.

The results shown in Figs. 2 and 3 clearly show that the employed numerical solution algorithm leads to a fairly good agreement with experimental and numerical data of other authors.

**Results of numerical modeling**

As the phase change material, the *n*-octadecane with the following characteristics was considered: $\rho_m$ = 746 kg/m$^3$, $\rho_s$ = 814 kg/m$^3$, $\beta = 8.5\cdot10^{-4}$ K$^{-1}$, $\mu = 1.81\cdot10^{-3}$ kg/(m·s), $\lambda_m$ = 0.157 W/(m·K), $\lambda_s$ = 0.39 W/(m·K), $T_m$ = 301 K, $L_m = 2.41\cdot10^5$ J/kg, $C_m$ = 2200 J/(kg·K), $C_s$ = 1900 J/(kg·K). Numerical investigations have been conducted at the following values of determining parameters: $4\cdot10^5 \le \mathrm{Ra} \le 5\cdot10^7$, $2.21 \le \mathrm{Ste} \le 5.53$, and Pr = 48.36, which are due to the analysis of the influence of the enclosure size and temperature head on flow structure and heat transfer. The enclosure size was varied from 1 to 5 centimeters, and the temperature head was varied from 10 to 50 °C.

As was noted above, the heat is transferred inside the region under consideration besides the conductive mechanisms at the expense of the formation of convective flows arising in the melted material. The melt circulation has contributed to an accelerated melting and a more intense energy transfer from the source.

The contours of the stream function $\Psi$ and temperature $\Theta$ at $\mathrm{Ra} = 4\cdot10^5$ and Ste = 5.53 at different moments of time are shown in Fig. 4. The phase change boundary is depicted in the figures by a solid line in the distributions of streamlines and by the isotherm $\Theta = 0$ in the distributions of temperature isolines. It is to be noted that at the initial time stage at $\tau \le 244.8$ (Fig. 4*a*), the heat conduction is the determining mechanism of heat transfer in the melt zone, which is confirmed by a uniform distribution of isotherms in this region. At the subsequent moments of time, a thermal plume forms above the energy source and, respectively, a more intense melting of the material occurs in the vertical direction because of the intensification of the convective mechanism of energy transfer. The recirculation flow is characterized independently of time by two convective cells, which indicate the presence of an ascending flow directly above the heat-releasing element and two descending flows along the phase change boundary. With increasing $\tau$ the cores of convective cells shift in the vertical direction, which is explained by a flow intensification inside the melt zone: $|\Psi|_{\max}^{\tau=244.8} = 0.0007 < |\Psi|_{\max}^{\tau=489.6} = 0.0018 < |\Psi|_{\max}^{\tau=734.4} = 0.003 < |\Psi|_{\max}^{\tau=1713.6} = 0.0055$. By the moment of time $\tau = 1713.6$ (Fig. 4*d*), the boundary of melting reaches the upper adiabatic wall in the presence of a pronounced thermal plume inside the melt. Starting from this time moment, an intense melting of the material realizes in the transverse direction. It is to be noted that at $Y = 0$, the motion of the melting front in the horizontal direction in the time range under consideration is insignificant due to the domination of the conduction mechanism of heat transfer

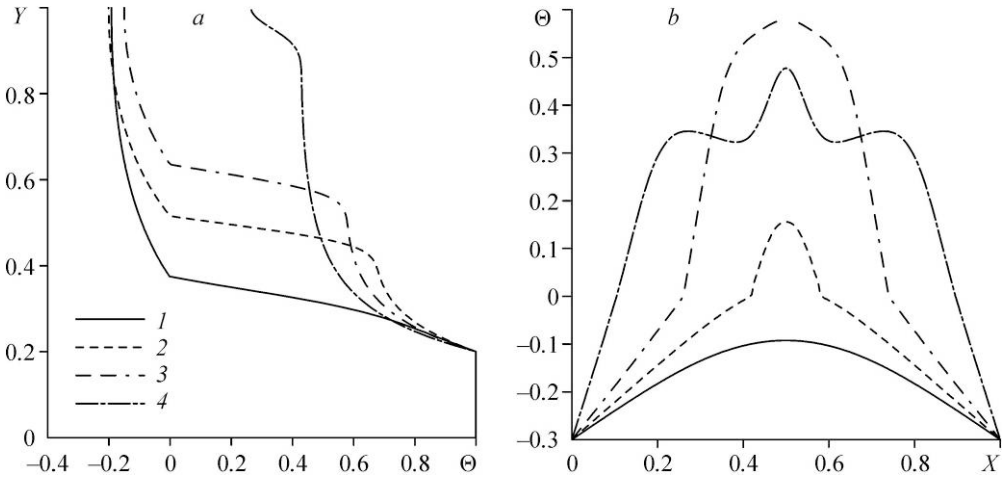


*Fig. 5.* Temperature Θ profiles in sections $X = 0.5$ (*a*) and $Y = 0.5$ (*b*) at $\mathrm{Ra} = 4 \cdot 10^5$ and $\mathrm{Ste} = 5.53$ at different moments of time. $\tau = 244.8$ (*1*), 489.6 (*2*), 734.4 (*3*), 1713.6 (*4*).

in the neighborhood of the energy source and reaching some thermal equilibrium with the heat flux on the side of cooling vertical walls.

Detailed temperature distributions in sections $X = 0.5$ and $Y = 0.5$ as well as of the vertical velocity component in section $Y = 0.5$ are shown in Figs. 5 and 6*a*.

Analyzing the temperature distributions one can note that with increasing time, the most intense heating and, respectively, the melting occur in the cavity central part. Directly above the energy source ($0.2 < Y < 0.3$), one observes even a temperature diminution at $\tau = 1713.6$ as compared to the initial time stage $\tau \le 244.8$, which is due to an intense convective flow and cooling of the melt descending flows on the side of the material being in solid state. Such a trend is observed also at a larger distance from the heat-releasing element. One should note a temperature drop in the upper part of the object under analysis ($Y > 0.8$) for two moments of time $\tau = 244.8$ and $\tau = 489.6$, which is due to different velocities of the advancement of the low-temperature wave from the vertical walls and the material melting on the energy source side.

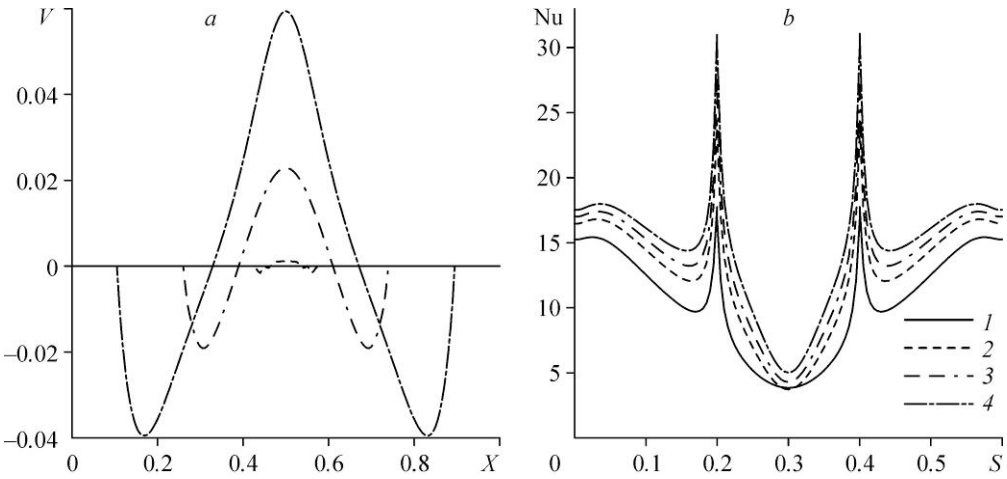


*Fig. 6.* Profiles of the vertical velocity component $V$ in section $Y = 0.5$ (*a*) and the local Nusselt number along the energy source surface (*b*) at $\mathrm{Ra} = 4 \cdot 10^5$ and $\mathrm{Ste} = 5.53$ at different moments of time. See the notations in Fig. 5.

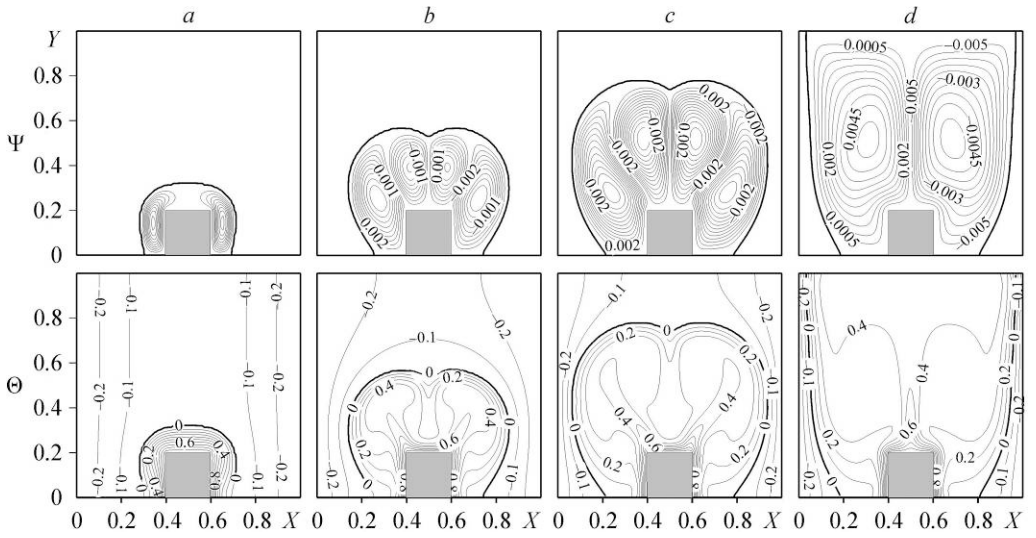


*Fig. 7.* Streamlines Ψ and isotherms Θ at Ra = $10^6$ and Ste = 2.21.
$\tau$ = 77.4 ( *a*), 387 (*b*), 774 (*c*), 1935 (*d*).

The noted intensification of the convective mechanisms of energy transfer in the cavity upper part, which is reflected in the temperature decrease near the source, is presented in Fig. 5*b*, where one can see a significant pressure drop in section $Y = 0.5$ with increasing dimensionless time from $\tau = 734.4$ to $\tau = 1713.6$. A symmetric distribution of streamlines and isotherms (Fig. 4, 5*b*) is due to the symmetry of boundary conditions and moderate values of the determining parameters (the Rayleigh and Stefan numbers).

The profiles of the vertical velocity component in section $Y = 0.5$ (Fig. 6*a*) show both the melt zone sizes and the dominance of the vertical direction of melting process as compared to the transverse one. One should also note the commensurable intensity of descending flows with the ascending flow, which is just a reason for the temperature decrease even in the cavity central part with increasing time (Fig. 5*b*).

The temporal dependence of the local Nusselt number $\left(\mathrm{Nu} = \left|\partial\Theta/\partial\overline{n}\right|\right)$ along the source surface is shown in Fig. 6*b*. One observes with increasing $\tau$ an increase in the local dimensionless heat-transfer coefficient. A drop of Nu on the source upper wall as compared to the side boundaries is due to the thermal plume formation and, respectively, a more intense heating in this zone, which leads to a temperature gradient decrease. A symmetric distribution of all parameters under consideration with respect to the axis $X = 0.5$ is reflected in the coincidence of the values of mean Nusselt numbers on the vertical walls of the energy source.

An increase in the temperature head by the factor of 2.5 leads to a growth of the Rayleigh number and decrease in the Stefan number, which manifests itself in a significant modification of the distributions of stream function and temperature contours (Fig. 7). One should note a high intensity of the melting process as compared to the lower temperature head, which is confirmed by a considerable advancement of the melting front. At the initial time stage at $\tau \le 77.4$ (Fig. 7*a*), the heat conduction is also a determining mechanism of energy transfer, and the formed hydrodynamic structure does not differ from the case presented above in Fig. 4*a*. The time increase leads to the development of two temperature plumes near the corner points of the energy source, which is evidenced by the appearance of two extra recirculation flows directly above the heat-releasing element. Such a distribution of streamlines characterizes the formation of an ascending flow along the axis of each thermal plume and three descending flows along the symmetry axis of the object under analysis and along the melting front.

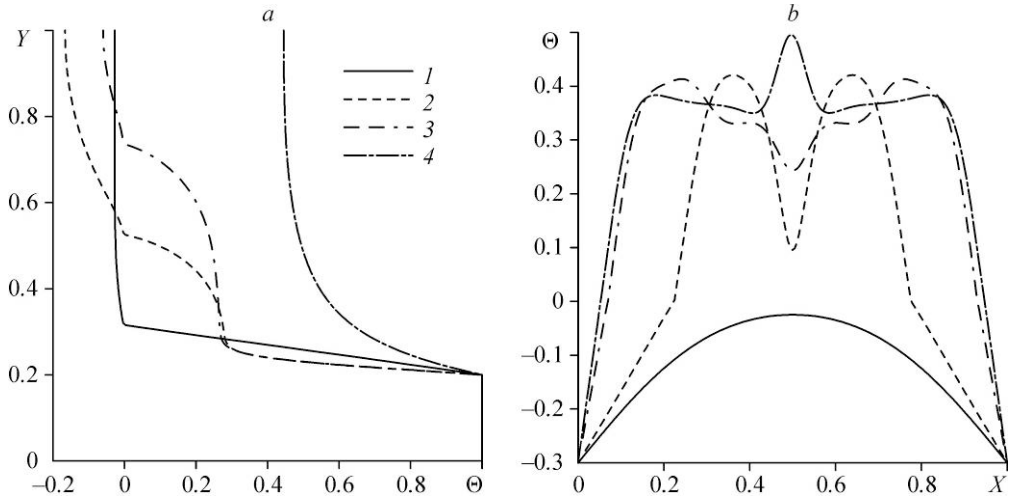


*Fig. 8.* Temperature Θ profiles in sections $X = 0.5$ (*a*) and $Y = 0.5$ (*b*) at Ra = $10^6$ and Ste = 2.21 at different moments of time.
$\tau = 77.4$ (*1*), 387 (*2*), 774 (*3*), 1935 (*4*).

One should pay attention to a significant difference from the foregoing melting regime (Fig. 4), which is expressed by a more intense melting of the material also in the transverse direction. The descending flow along the symmetry axis characterizes the formation of a low-temperature plume on the solid material side. In the time interval from $\tau = 774$ to $\tau = 1935$, there occurs the merging of two thermal plumes into a single one and, respectively, the formation of only two convective cells of equal intensity, which show the melt motion in the clockwise and counter-clockwise directions.

Figures 8 and 9*a* show the profiles of temperature Θ in sections $X = 0.5$ and $Y = 0.5$ as well as the vertical velocity component $V$ in section $Y = 0.5$ at Ra = $10^6$ and Ste = 2.21. Unlike the foregoing melting regime, a less significant growth of temperature in the range from 0 to 0.2 also occurs in the enclosure central part. One observes here a considerable reduction of Θ immediately above the energy source with increasing time, which is due to the formation of a central descending melt flow. A complex structure of the temperature and velocity fields is

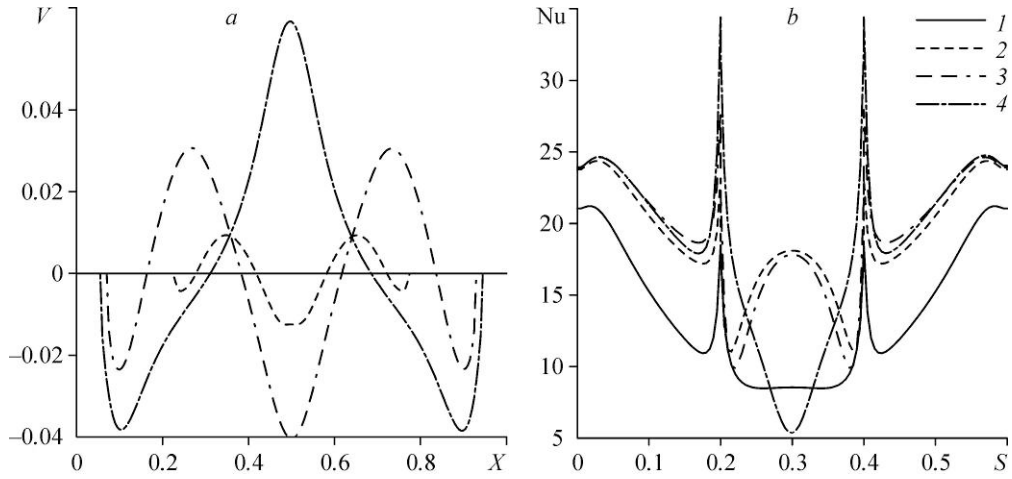


*Fig. 9.* Profiles of the vertical velocity component $V$ in section $Y = 0.5$ (*a*) and the local Nusselt number along the energy source surface (*b*) at Ra = $10^6$ and Ste = 2.21 at different moments of time.
See notations in Fig. 8.

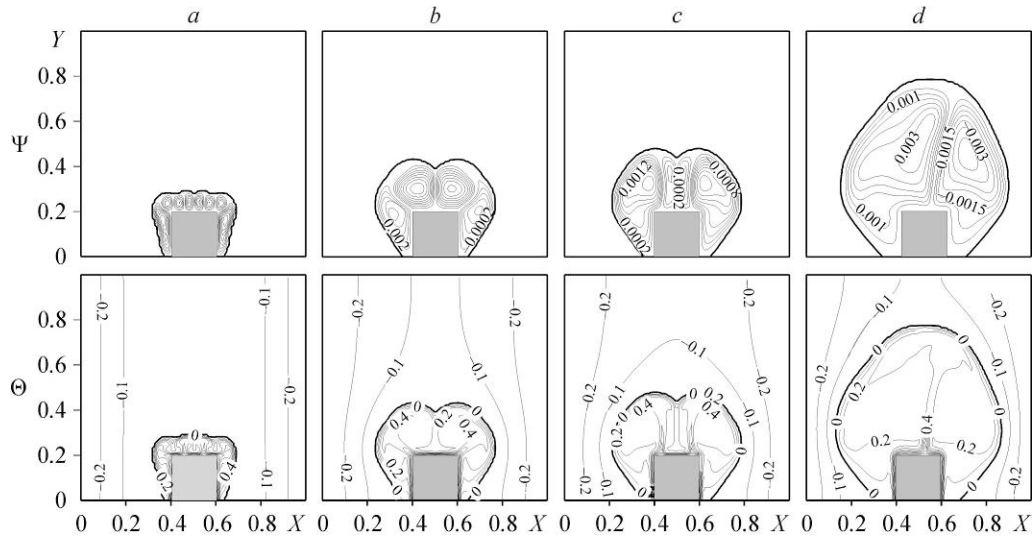


*Fig. 10.* Streamlines Ψ and isotherms Θ at Ra = $5 \cdot 10^7$ and Ste = 5.53.
$\tau$ = 329.4 (*a*), 1098 (*b*), 1427.4 (*c*), and 3843 (*d*).

confirmed by the Θ and *V* profiles in section $Y = 0.5$ (Fig. 8*b* and 9*a*), where the location of two thermal plumes is depicted, which merge by the moment of time $\tau = 1935$. One should also pay attention to an insignificant transverse heating of the material at the variation of $\tau$ from 774 to 1935, which manifests itself in a substantial reduction of the transverse velocity of the material melting (Fig. 9*a*).

The most significant variations of the local Nusselt number occur on the sidewalls of the energy source at the time variation in the range from $\tau = 77.4$ to $\tau = 387$ (Fig. 9*b*). The appearance of two thermal plumes and, respectively, of the central descending flow manifests itself in an increase of the Nusselt number on the heater upper surface because of the temperature gradient growth. The formation of a single central temperature plume leads to a decrease in the local Nusselt number along the entire upper wall of the energy source.

A fivefold increase in the enclosure size leads to a growth of the Rayleigh number under the constancy of the Stefan number, which manifests itself, as at the temperature head increase, in a significant modification of the flow structure and the temperature field (Fig. 10). In this case, the Rayleigh number inside the melt zone reaches the value $5 \cdot 10^7$, which assumes the formation of a highly intense convective flow. It is to be noted that the growth of the Rayleigh number not only leads to the alteration of the flow structure inside liquid phase but also, as a consequence, affects the shape of the interphase boundary. The flow complicates substantially, the formation of two thermal plumes is observed with increasing temperature head, which shift with time to the upper wall center and merge. At the expense of the appearance of two thermal plumes and additional recirculation flows, the melting above the source occurs uniformly both in the vertical and horizontal directions. With the melt zone growth the temperature plume starts oscillating, and the flow pattern becomes asymmetric. Such an alteration is due to the predominance of the buoyancy force over the internal forces, which just manifests itself in the formation of an asymmetric flow pattern and heat transfer.

The detailed profiles of temperature and velocity in mid-sections $X = 0.5$ and $Y = 0.5$ of the object under analysis are presented in Figs. 11 and 12*a*. The observed changes confirm completely the above-described peculiarities, which are due to a significant growth of the lift magnitude. The appearance of two temperature plumes and their evolution in the process of melting is reflected in the non-uniformity of the local Nusselt number distributions (Fig. 12*b*).

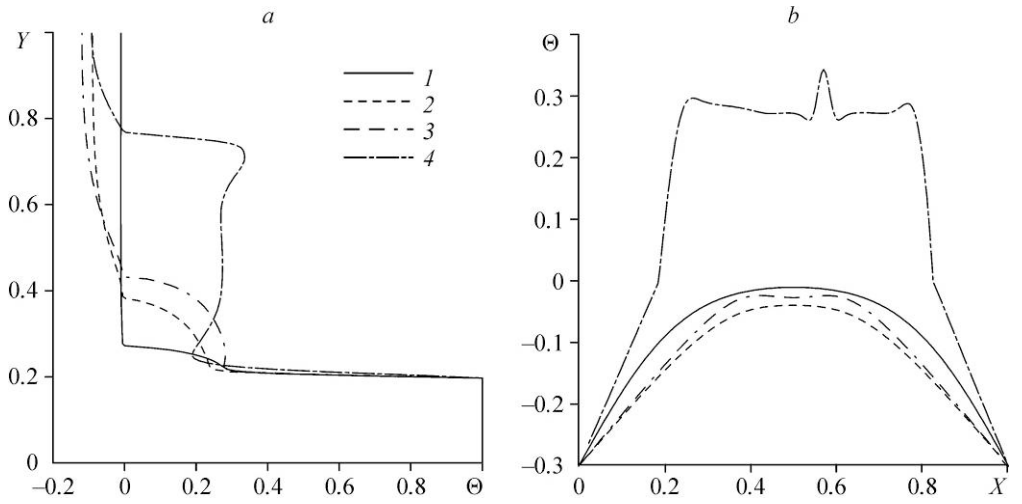


*Fig. 11.* Profiles of temperature Θ in sections $X = 0.5$ (*a*) and $Y = 0.5$ (*b*) at $Ra = 5 \cdot 10^7$ and $Ste = 5.53$ at different moments of time.
$\tau$ = 329.4 (*1*), 1098 (*2*), 1427.4 (*3*), and 3843 (*4*).

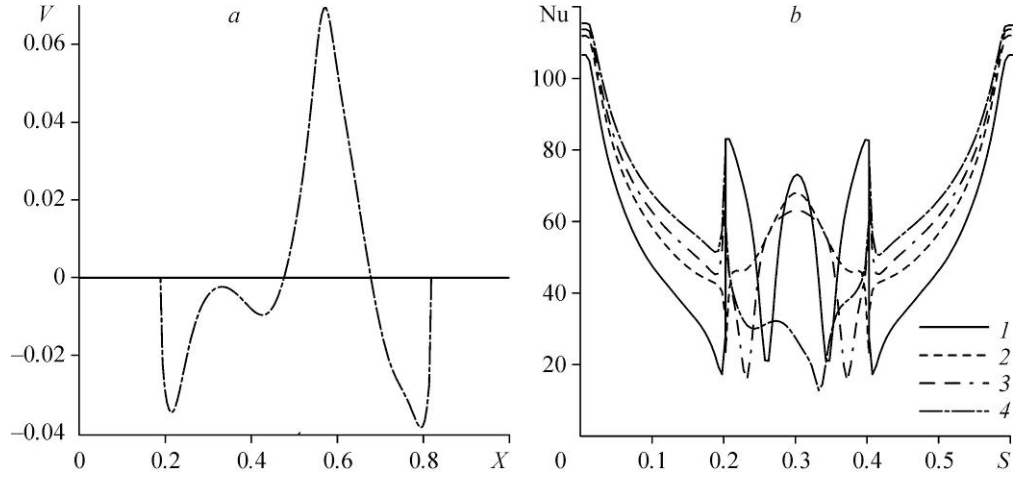


*Fig. 12.* Profiles of the vertical velocity component $V$ in the section $Y = 0.5$ (*a*) and the local Nusselt number along the energy source surface (*b*) at $Ra = 5 \cdot 10^7$ and $Ste = 5.53$ at different moments of time.
See notations in Fig. 11.

## Conclusion

The unsteady problem of the material melting inside a closed square cavity with isothermal vertical walls in the presence of a local energy source has been solved numerically. The distributions of the stream function and temperature contours, the temperature and velocity profiles in the mid-sections of the solution domain as well as the local Nusselt number profiles along the energy source surface, which illustrate the influence of determining complexes ($4 \cdot 10^5 \le$ $\le Ra \le 5 \cdot 10^7$, $2.21 \le Ste \le 5.53$) on the flow structure and heat transfer have been presented. It has been found that an increase in the Rayleigh number manifests itself in a substantial complication of fluid dynamics and heat transfer of the process: one observes the formation of two

temperature plumes, which merge with increasing time. It has been found that an asymmetry is possible in the distributions of local structures at a substantial domination of the buoyancy force over the internal forces of friction. It has been shown that a reduction of the local Nusselt number on the upper wall of the energy source is due to the heating of the melt zone above the heater and, respectively, the temperature gradient reduction. In the case of the formation of two temperature plumes, a central descending flow arises between them, which leads to a local growth of the Nusselt number on the upper wall of the heat-releasing element.

## References


1. **S. Raoux and M. Wutting,** Phase Change Materials. Science and Applications, Springer, Berlin, 2009.
2. **C. Gau and R. Viskanta,** Melting and solidification of pure melting on a vertical wall, ASME J. Heat Transfer, 1986, Vol. 108, P. 174–181.
3. **Z.-X. Gong and A.S. Mujumdar,** Flow and heat transfer in convection-dominated melting in a rectangular cavity heated from below, Int. J. Heat Mass Transfer, 1997, Vol. 41, P. 2573–2580.
4. **T. Kousksou, M. Mahdaoui, A. Ahmed, and A.A. Msaad,** Melting over a wavy surface in a rectangular cavity heated from below, Energy, 2014, Vol. 64, P. 212–219.
5. **H.F. Oztop, E. Abu-Nada, Y. Varol, and A. Chamkha,** Natural convection in wavy enclosures with volumetric heat sources, Int. J. Thermal Sci., 2011, Vol. 50, P. 502–514.
6. **W. Shyy and M.-H. Chen,** Steady-state natural convection with phase change, Int. J. Heat Mass Transfer, 1990, Vol. 33, P. 2545–2563.
7. **F.L. Tan and C.P. Tso,** Cooling of mobile electronic devices using phase change materials, Appl. Thermal Engng, 2004, Vol. 24, P. 159–169.
8. **S.C. Fok, W. Shen, and F.L. Tan,** Cooling of portable hand-held electronic devices using phase change materials in finned heat sinks, Int. J. Thermal Sci., 2010, Vol. 49, P. 109–117.
9. **X. Sun, Q. Zhang, M.A. Medina, and S. Liao,** Performance of a free-air cooling system for telecommunications base stations using phase change materials (PCMs): in-situ tests, Applied Energy, 2015, Vol. 147, P. 325–334.
10. **Y.-H. Wang and Y.-T. Yang,** Three-dimensional transient cooling simulations of a portable electronic device using PCM (phase change materials) in multi-fin heat sink, Energy, 2011, Vol. 36, P. 5214–5224.
11. **Y.-T. Yang and Y.-H. Wang,** Numerical simulation of three-dimensional transient cooling application on a portable electronic device using phase change material, Int. J. Thermal Sci., 2012, Vol. 51, P. 155–162.
12. **S.G. Martyushev and M.A. Sheremet,** Numerical analysis of the convection-radiation heat transfer in a closed air cavity with local heat source, Komputernye issledovaniya i modelirovanie, 2014, Vol. 6, No. 3, P. 383–396.
13. **Y. Belhamadia, A.S. Kane, and A. Fortin,** An enhanced mathematical model for phase change problems with natural convection, Int. J. Numer. Anal. and Modeling, Series B, 2012, Vol. 2, P. 192–206.
14. **V.F. Strizhov (Ed.).** Numerical Investigations of Natural Convection Flows of Solidifying Liquid. Trudy IBRAE RAN (general editor L.A. Bolshov), issue 2, Nauka, Moscow, 2007.
15. **N.S. Bondareva and M.A. Sheremet,** Study of melting of a pure gallium under influence of magnetic field in a square cavity with a local heat source, IOP Conf. Series: Materials Sci. and Engng, 2015, Vol. 93, P. 012004-1–012004-6.
16. **N.S. Bondareva and M.A. Sheremet,** Numerical simulation of melting of a pure gallium in a rectangular enclosure, in: Proceedings of XII Int. Conf. of students and young scientists "Prospects of Fundamental Sciences Development Tomsk Polytechn. Univ., Tomsk, 2015, P. 627–629.
17. **S.G. Martyushev and M.A. Sheremet,** Conjugate natural convection combined with surface thermal radiation in an air filled cavity with internal heat source, Int. J. Thermal Sci., 2014, Vol. 76, P. 51–67.
18. **V.M. Paskonov, V.I. Polezhaev, and L.A. Chudov,** Numerical Modeling of Heat and Mass Exchange Processes, Nauka, Moscow, 1984.